Combined Application of RGB Marking and Mass Spectrometric Imaging Facilitates Detection of Tumor Heterogeneity

PIERRE ABRAMOWSKI[1*], OLGA KRAUS[2*], SASCHA ROHN[3], KRISTOFFER RIECKEN[1], BORIS FEHSE[1#] and HARTMUT SCHLÜTER[2#]

[1]*Research Department of Cell and Gene Therapy, Department of Stem Cell Transplantation, and*
[2]*Mass Spectrometric Proteome Analysis, Department of Clinical Chemistry and Laboratory Medicine, University Medical Center Hamburg-Eppendorf, Hamburg, Germany;*
[3]*Hamburg School of Food Science, Institute of Food Chemistry, University of Hamburg, Hamburg, Germany*

Abstract. *Cancer-cell heterogeneity dramatically influences treatment success, but escapes detection by classical histology. Mass-spectrometric imaging (MSI) represents a powerful method for visualizing the spatial distribution of proteins in tissue sections. Herein we asked whether MSI also facilitates detection of tumor heterogeneity. We first transduced the human neuroendocrine-carcinoma BON cell line following the red-green-blue (RGB) marking principle. RGB marking allows for specific color-coding of individual clones. Mice transplanted with RGB-marked BON cells developed liver tumors. We identified 16 primary tumors clearly distinguishable by histology and fluorescence imaging, but also based on a common tumor-specific signal pattern detected by MSI. Importantly, this pattern was clearly confined to tumor tissue while was absent from surrounding liver tissue. At the same time, we observed protein signals differentially present in a few or even single tumors. Since these signals were independent of RGB marking, they apparently reflected unique intrinsic protein-signal patterns of individual tumors. Thus, our data propose MSI as a tool for identifying divergent tissue by 'fingerprints' of protein signals, allowing not only for differentiation of tumor from healthy tissue but also detection of tumor heterogeneity. In conclusion, by visualizing tumor heterogeneity, MSI ideally complements microscopy-based methods. This might help to better understand tumor biology and develop future treatment strategies.*

*Equal first authors; #equal last authors.

Correspondence to: Professor Dr. Boris Fehse, Research Department Cell and Gene Therapy, Department of Stem Cell Transplantation, University Medical Center Hamburg-Eppendorf, Martinistr. 52, 20246 Hamburg, Germany. Tel: +49 40741055518, Fax: +49 40741055468, e-mail: fehse@uke.de and Professor Dr. Hartmut Schlüter, Mass Spectrometric Proteome Analysis, Department of Clinical Chemistry & Laboratory Medicine, University Medical Center Hamburg-Eppendorf (UKE), Martinistr. 52, Hamburg, 20246, Germany. Tel: +49 40741058795, Fax: +49 40741040097, e-mail: hschluet@uke.de

Key Words: Mass spectrometric imaging, MSI, tumor heterogeneity, RGB marking, proteomics, lentiviral vectors.

It is well-accepted that assessing the spatial distribution of peptides and proteins in cancer tissue provides important insights into cancer biology, and thus may aid us in identifying novel biomarkers and target structures for targeted-therapies (1). Moreover, variable patterns of protein and peptide levels in different areas of one and the same tumor can help uncover intratumoral heterogeneity, as was recently shown by Balluff *et al.* (2).

Mass spectrometric imaging (MSI) has been suggested as a promising method for analyzing the spatial distribution of proteins and peptides (3, 4), lipids (5, 6) and small molecules, including exogenous drugs (7) and their metabolites (8) in various tissues. Based thereon, MSI has also been used for disease biomarker screening (9).

MSI has certain advantages supporting its use for the analysis of tumor tissue. Sample preparation is rather simple and includes a few washing steps of the tissue sections and subsequent application of matrix-assisted laser desorption ionization (MALDI) matrix onto the surface of the section. In the MALDI mass spectrometer, every grid of the section is irradiated by the MALDI laser, generating one mass spectrum for each pixel. MSI images for defined m/z values are generated by algorithms that result in maps of defined signal intensities, thereby displaying the spatial distribution of relative amounts of a defined biomolecule (10).

At the same time, there exist specific limitations to MSI. Although it allows the detection of many dozens of different peptides and proteins in tissue sections, typically only 300

to 1,000 distinct mass signals are detected (4), representing only a small fraction of the total number of existing molecules. Indeed, there are more than 10,000-12,000 ubiquitously expressed proteins in a single cell but some of these do not produce any peptides if using trypsin, or they are not mass spectrometry-compatible because of their physicochemical properties (11).

We recently established a novel cell-marking approach, namely red-green-blue (RGB) marking, based on the stable integration of gene-transfer vectors into the genome of transduced cells (12, 13). To do so, we used three different lentiviral LeGO vectors (14) that encoded the red fluorescent protein (FP) mCherry, the yellow-green FP Venus, and the blue FP Cerulean, respectively. Combined transduction with all three vectors at equal multiplicities of infection (MOIs) resulted in a mixture of cells expressing none, one, two or all three different FPs. Consequently, individual transduced cells were marked either by one of the three basic colors red (R), green (G), or blue (B), or, based on the additive RGB color model by any possible color hue resulting from their combination. Importantly, we showed that color coding of individual cell clones was stable over time and even upon serial transplantation (12).

In the present study, we aimed to investigate the applicability of MSI in (i) assessing protein patterns in different tumors and (ii) visualizing tumor clonality, as well as heterogeneity. We made use of an established tumor model in non-obese diabetic severe combined immunodeficient (NOD-SCID) mice (15, 16), which developed liver tumors after infusion of RGB-marked human carcinoid cells (12, 13). We show that both techniques, MSI and RGB marking, are complementary and thus in combination represent helpful tools for cancer research.

Materials and Methods

Ethics statement. All animal experiments were approved by local authorities (Behörde für Soziales, Gesundheit und Verbraucherschutz Hamburg, ref. no.: G09/39) and performed in accordance with relevant guidelines and regulations for animal welfare.

Production of lentiviral vector particles. The three lentiviral vectors LeGO-C2 (encoding the red fluorescent protein mCherry (17)), LeGO-V2 (yellow-green, Venus (18)) and LeGO-Cer2 (blue, Cerulean (19)) are described elsewhere (12, 13). Infectious lentiviral-vector particles were generated as previously described (12, 13). Briefly, 5×10^6 HEK293T cells were seeded in HEK293T medium [Dulbecco's modified eagle medium (DMEM), high glucose, GlutaMAX-I supplement, pyruvate (Gibco, Carlsbad, CA, USA), 10% fetal calf serum (FCS), 1 mM sodium pyruvate (Gibco), 20 mM HEPES (Gibco), 1% vol/vol of 10,000 U/ml penicillin and 10,000 μg/ml streptomycin (Gibco), respectively] into 9-cm petri dishes at day 1. The next day, the medium was changed to HEK293T medium supplemented with 25 μM chloroquine. Cells were transfected with a mixture of 10 μg vector plasmid, packaging plasmids (10 μg pMDLg/pRRE, 5 μg pRSV-rev, 2 μg pHCMV-VSV-G) and 0.25 M calcium chloride in 500 μl H_2O. Plasmid mixtures were added drop-wise to equal volumes of 2× HBS buffer (pH 7.15) before addition to HEK293T cultures. After incubation for 6-8 h, the medium was changed to HEK293T medium. Twenty-four hours later (day 3), supernatants were filtered through 45 μm filters and stored at −80˚C. Viral particles were titrated by seeding 5×10^4 HEK293T into 24-well plates (Greiner Bio-One, Frickenhausen, Germany) in 500 μl HEK293T medium. After cells became adherent, 8 μg/ml polybrene as well as 10-fold dilutions of viral particle-containing supernatant were added prior to centrifugation (1000×g, 25˚C, 1 h). The medium was changed the next day, and transduction rates were determined 48 h later on a FACSCanto II (407, 488, 633-nm lasers) flow cytometer (BD Biosciences, San Jose, CA, USA). Titers were calculated considering only wells containing 5-30% transduced cells (20).

RGB marking of BON cells. The human neuroendocrine carcinoma cell line BON (21) was cultured in BON medium (DMEM/F12 (Gibco) supplemented with 10% FCS, 1% vol/vol of 10,000 U/ml penicillin and 10,000 μg/ml streptomycin, respectively, and 2 mM L-glutamine (Gibco). For RGB marking 5×10^4 cells were seeded into 24-well plates (Greiner) in 500 μl BON medium. Transduction was performed as described before to obtain gene-transfer efficiencies of 50-70% per vector (20). Frequencies of RGB-marked BON cells were assessed on an LSRFortessa (405, 488, 561, 640-nm lasers) flow cytometer (BD Biosciences).

Mice. NOD-SCID mice were bred by the animal facility of the University Medical Center Hamburg Eppendorf and housed in individually ventilated cage racks.

Transplantation of BON cells. RGB-marked BON cells were transplanted into recipient mice, as published earlier (12). Briefly, 5×10^4 BON cells suspended in 200 μl DMEM with 2% FCS were injected intrasplenically into NOD-SCID mice anesthetized by intraperitoneal injection of ketamine-xylazine. In some experiments, we splenectomized mice after cell injection. After transplantation, 0.2 mg enrofloxacine (Bayer, Leverkusen, Germany) per mouse were injected subcutaneously. Mice were killed 2 to 3 weeks after transplantation.

Fluorescence imaging. Prepared, non-fixed liver tissue was embedded in Tissue-Freezing Medium (Jung, Leica Biosystems, Nussloch, Germany) and frozen in isopentane (Carl Roth, Karlsruhe, Germany). Tissue was stored at −80˚C. Slices of 6 μm were generated using a cryostat and mounted on glass microslides (Superfrost/Plus, Karl Hecht, Sondheim, Germany). Images were acquired using an IX81 inverted microscope (Olympus, Hamburg, Germany) and analyzed with cell^P 3.4 software (Olympus Soft Imaging Solutions, Münster, Germany). Images were stitched with Image Composite Editor 2.0.2.0 (Microsoft, Redmond, WA, USA).

Sample preparation and matrix deposition for MSI. The frozen mouse liver tissue was sliced into 6 μm thick sections using a microtome (Microm HM 355, Thermo Fisher Scientific, Walldorf, Germany). The sections were deposited onto indium-tin-oxide (ITO)-coated glass slides (Bruker Daltonics, Bremen, Germany) which had been previously coated with polylysine. The slides were washed twice in 70% ethanol (HPLC grade, Merck, Darmstadt,

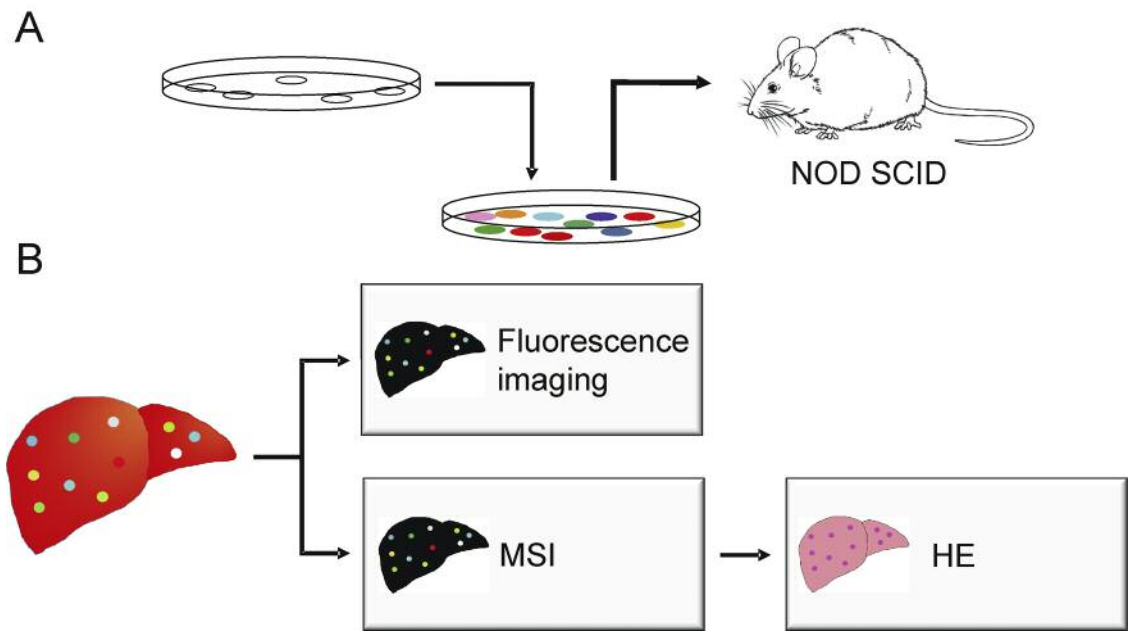

Figure 1. *Schematic depiction of the experimental set-up. A: BON cells were labeled by red-green-blue (RGB) marking and expanded in vitro before intrasplenic transplantation into non-obese diabetic severe combined immunodeficient (NOD-SCID) recipient mice. B: Engraftment of tumor cells was assessed by histology and fluorescence microscopy. Analysis was complemented by mass spectrometric imaging (MSI).*

Germany) and twice and in 100% ethanol for 1 min and allowed to dry. To obtain digital images of the mouse liver tissue, each slide was scanned using a flatbed scanner before matrix deposition. A droplet of a peptide and protein standard (Peptide & Protein Calibration Standard for MALDI, Bruker Daltonics) was placed at a blank position on the slide prior to matrix application to calibrate the mass spectrometer. The matrix solution was prepared by dissolving 200 mg sinapinic acid (Bruker Daltonics) in 20 ml of 60% acetonitrile (Merck, Darmstadt, Germany) and 0.2% trifluoroacetic acid (Sigma-Aldrich, Steinheim, Germany) to obtain a final matrix concentration of 10 g/l. The matrix was applied using an ImagePrep device. The spraying technique enabled full-matrix coverage over the entire tissue surface and facilitated co-crystallization of matrix and biomolecules. After matrix deposition, mouse liver tissue section was investigated by MSI.

MSI data acquisition and analysis. Mass spectra were acquired using an autoflex speed MALDI-TOF mass spectrometer (Bruker Daltonics) equipped with a smartbeam II laser. The mass spectrometer was controlled with the flexControl 3.3/flexImaging 3.0 software package (Bruker Daltonics). Spectra were acquired in positive linear mode in a mass-per-charge (m/z) range of 2-21 kDa and at a sampling rate of 1.0 GS/s. A total of 500 single spectra per pixel at a laser shot frequency of 1000 Hz at constant laser power were accumulated. Each spot position was systematically analyzed row by row to sample the entire spot area at a raster width of 160 μm. Data analysis and image generation was done with flexImaging 3.0. The total ion current of each spectrum was used for signal intensity normalization. Relevant signals that showed different distribution patterns in the mouse liver tissue compared to the human cancer cells were identified manually.

Histology. Subsequent to the MSI analysis, slides were rinsed in 100% xylene for 5 min in order to remove the matrix, and stained with hematoxylin and eosin (HE, both from Sigma-Aldrich). Microscopic images were generated using an automated slide scanner (Mirax Scan, Carl Zeiss, Göttingen, Germany) in order to spatially relate the peak intensities to histological structures.

Results

Experimental setup. To address the resolving power of MSI, we aimed to visualize tumors with this technique in direct comparison with two established methods, namely RGB marking and HE staining. We used an established animal model of liver-tumor formation based on transplantation of RGB-marked human carcinoid cells. The experimental outline is depicted in Figure 1.

Efficient RGB marking of BON cells in vitro. We first transduced human carcinoid BON cells with three LeGO vectors encoding FPs of the three basic colors red (mCherry, LeGO-C2), yellow-green (Venus, LeGO-V2), and blue (Cerulean, LeGO-Cer2) using equalized MOIs (Figure 2A). We obtained transduction rates of 50 to 70% for each of the three vectors (Figure 2B-D). Theoretically, genetic marking at these transduction rates can be expected to result in comparable frequencies (12.5% per group if transduced at a frequency of 50% per vector) of cells that were not transduced, transduced with one of three vectors, transduced

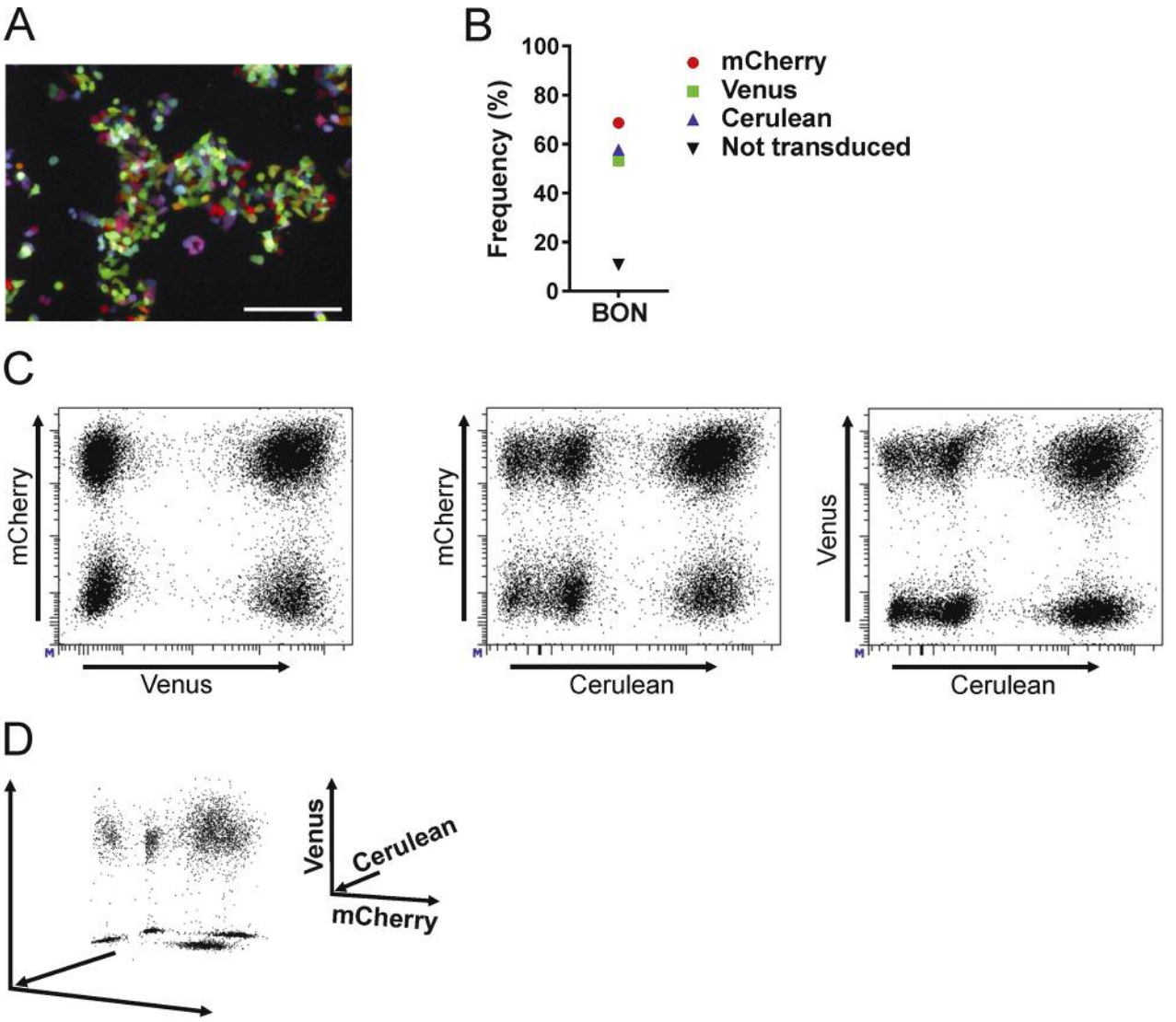

Figure 2. *Efficient red-green-blue (RGB) marking of BON cells. A: Fluorescence-microscopy image of RGB-marked BON cells. For RGB marking (12, 13) BON cells were simultaneously transduced with three different LeGO vectors encoding the fluorescence protein mCherry, Venus, and Cerulean, respectively. The scale bar represents 200 μm (magnification: ×10). B: Quantification of transduction efficiencies for the three individual fluorescence proteins by flow cytometry confirmed optimal RGB marking, as well as the presence of cells that remained non-transduced. C: Two-dimensional dot plots of RGB-marked BON cells analyzed by flow cytometry. The transduction procedure led to single-, double-, triple-, and non-transduced cells. Events are summarized in (D) in order to display the triple-positive cells.*

with two of the three vectors, or transduced with all three vectors (12, 13, 20). Indeed, approximately 10% of vector-exposed BON cells remained non-transduced (Figure 2B), while the remaining cells displayed a large variety of different colors, proving efficient RGB marking *in vitro* (Figure 2A, C and D).

RGB-marked BON cells form liver tumors. Next, polyclonal RGB-marked BON cells were transplanted into immune-deficient NOD-SCID mice. At sacrifice, 2 to 3 weeks after transplantation, livers of transplanted mice displayed the formation of multiple tumors (Figure 3). Based on the histological images the presence of tumor tissue in the liver sections was confirmed. As illustrated, BON-derived tumors can be easily distinguished from normal mouse liver tissue after HE staining in microscopic images. In contrast to surrounding liver tissue, tumor cells appeared as neoplastic with large nuclei resulting in characteristic purple staining patterns, and frequently displayed unstained, necrotic areas in their center (Figure 3A).

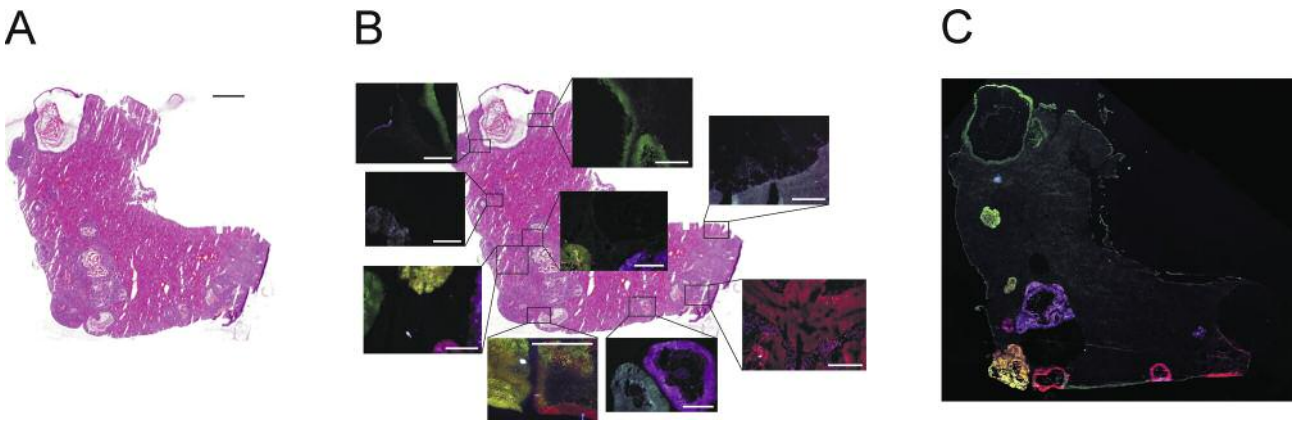

Figure 3. *Optical analysis of tumor formation and heterogeneity within liver tissue. A: Transplantation of red-green-blue (RGB) marked BON cells induced formation of multiple tumors in livers of recipient mice. B: Fluorescence imaging revealed that tumors were of different clonal origin as indicated by different colors, as well as the absence of color in some tumors. C: Different monoclonal tumors can also easily be distinguished in the overview of the whole liver lobe. Scale bars represent 2000 μm (magnification: ×20, black) and 500 μm (×4, white), respectively.*

Fluorescence images demonstrated outgrowth of homogenously colored, monoclonal tumors (Figure 3B, C) in accordance with previous data (12). As expected, not all tumor cells expressed fluorescence proteins, since only approximately 90% of the transplanted cells were RGB-marked (Figure 2B and D). Notably, non-RGB-marked tumors were readily-identified by histology (Figure 3A).

MSI images reveal different protein patterns in tumors. In the next step, we analyzed mouse liver tissue sections by MSI. To illustrate the differences of the individual tumors and the mouse liver tissue, the spectra of each tumor region and mouse liver tissue were compared. Figure 4 shows typical MSI spectra and highlights differences in the spectra, each summed over the individual areas. To illustrate differences we marked some of the signals unique for tumor cells or mouse tissue, respectively, by red asterisks. These include, among others, the signal 6667 m/z in tumor 16, 3713 m/z in tumor 15, 2808 m/z in tumor 10 and 8451 m/z in the mouse tissue. The black asterisks annotate peaks that were present in several tumor areas (5064 m/z, and 10,090 m/z).

For a better overview, m/z signals and their corresponding intensities of the summed mass spectra of each individual tumor area and of the mouse tissue area were converted into a density plot (Figure 5). All tumors shared several signals with the same m/z values (*e.g.* 9514 m/z; 10090 m/z; 11638 m/z) (Figure 6A). There were also clear differences between all tumors, which gave each single tumor an individual fingerprint highlighting their heterogeneity. For example, the signals 5064 m/z, 6823 m/z, 9431 m/z and 10604 m/z were detected only in some tumor regions. Signal 6823 m/z was measured in six tumor areas (Figure 6A). Some tumor areas contained unique signals, such as signal 6667 m/z, detected only in one tumor area (Figure 6B). In the mouse tissue, signals such as 14,168 m/z were present exclusively, and the spatial distribution of their signal intensities is quite homogeneous (Figure 6B).

Discussion

In the present work, we directly compared the ability of different visualization techniques to detect tumor tissue, namely standard histology, RGB marking and MSI. To do so, we made use of a previously described liver-tumor model based on RGB-marked BON cells (12).

Our study presents two main findings. Firstly, with regard to tumor detection we found a remarkable correlation between the three techniques. In fact, all tumors detected by histology and RGB marking were also easily revealed by MSI. Moreover, MSI allowed mapping even of those tumors, which were not transduced and therefore not RGB-marked by fluorescent proteins. Even considering the particularities of the given model system (xenogeneic neuroendocrine tumor in the liver), this data still suggests that MSI might be a very promising method for discriminating between different tissues, in particular healthy and malignant cells.

The second finding of our study, namely the detection of intertumoral heterogeneity by MSI 'fingerprints' (Figures 4 and 5), was even more intriguing. As was previously shown, RGB marking allows for clonal tracking of both normal and malignant cells (12, 22). Indeed, individual RGB-marked BON tumors in this study were uniformly colored indicating clonal outgrowth in line with previous results (12, 13). At the same time, different colors of discrete tumors specified heterogeneity with regard to clonal marking. However, unexpectedly our MSI data introduced an additional level of heterogeneity between individual clonal tumors not related to RGB marking. In fact, tumors marked with

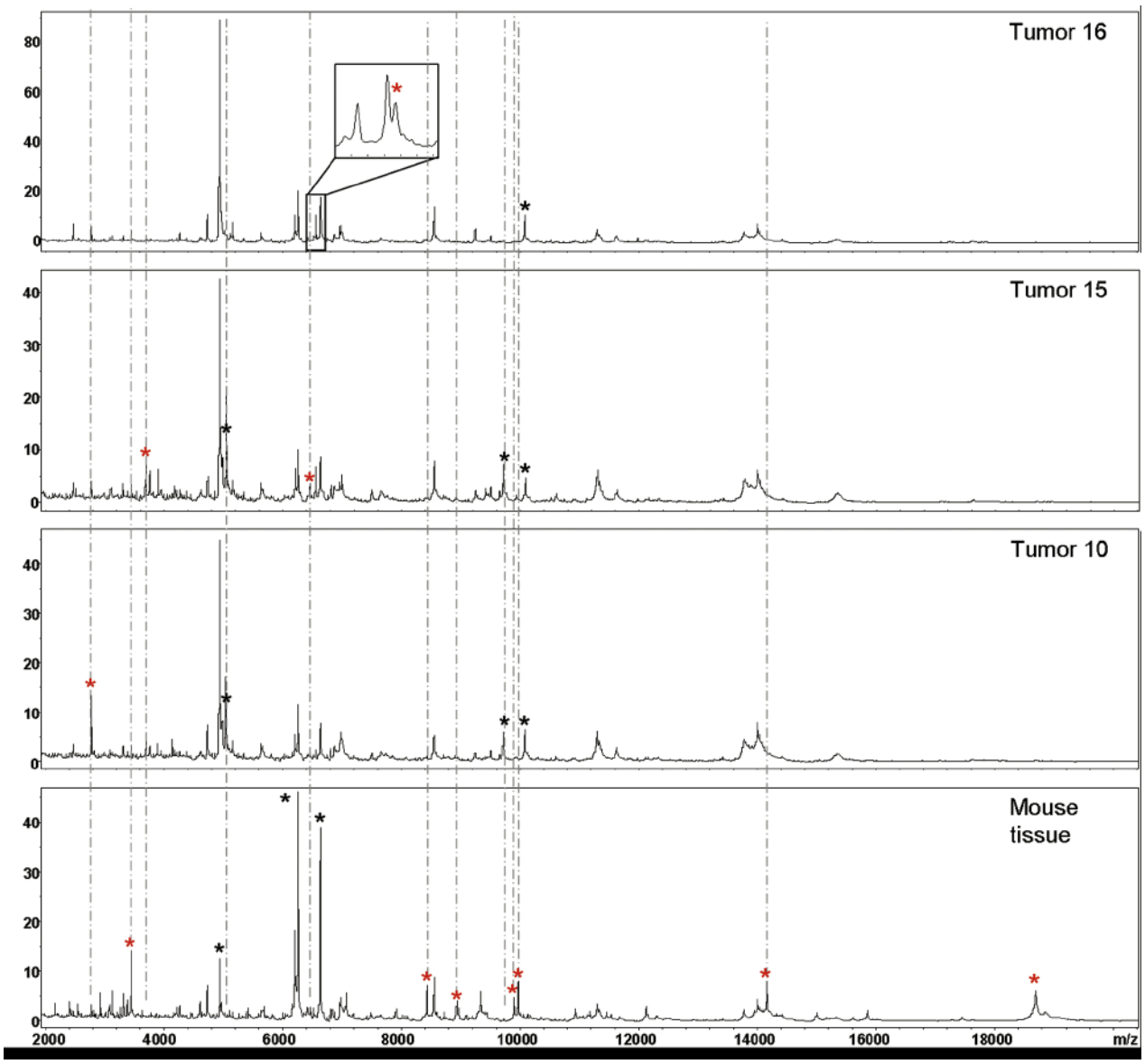

Figure 4. *Representative mass spectrometric imaging (MSI) spectra of three primary tumors and mouse liver tissue. A signal at 6669 m/z (annotated with red asterisk) was detected only in tumor 16, all other signals were also detected in tumor 15 and 10 (annotated with black asterisk). Additionally, tumor 15 contained unique signals at 3712 m/z and at 6471 m/z, and tumor 10 at 2803 m/z (annotated with red asterisk). The spectrum of mouse liver tissue consisted of several peaks, which were present only in the mouse tissue e.g. 3462 m/z and 9974 m/z (annotated with red asterisk).*

different fluorescent proteins, but even non-transduced tumors, exhibited specific protein signatures that were not related to the expressed fluorescent proteins. Our results, therefore, indicate that MSI, alone or in combination with RGB marking, may equip basic research with a novel combinatorial tool for assessing clonality and heterogeneity of solid tumors.

Characteristic protein patterns have been in focus for decades in the attempt to unravel and to delineate cancer tissue from normal healthy tissue. Specific molecules have been shown to be suitable discriminators for heterogeneous tissues and specific cell types (23). Candidate proteins proposed as biomarkers for malignant tissue of various origins have been identified by mass spectrometry, necessitating the extraction of proteins from biopsies (24). Whereas spatial dissemination as well as the relative abundance of a given protein are lost after tissue homogenization, tissue profiling by MSI is performed on intact tissue sections and thus spatial protein distributions can be detected (25). Consequently, application of MSI to detect areas of malignant cells in tissue sections without the necessity of using antibodies for tumor-cell detection was suggested (26,

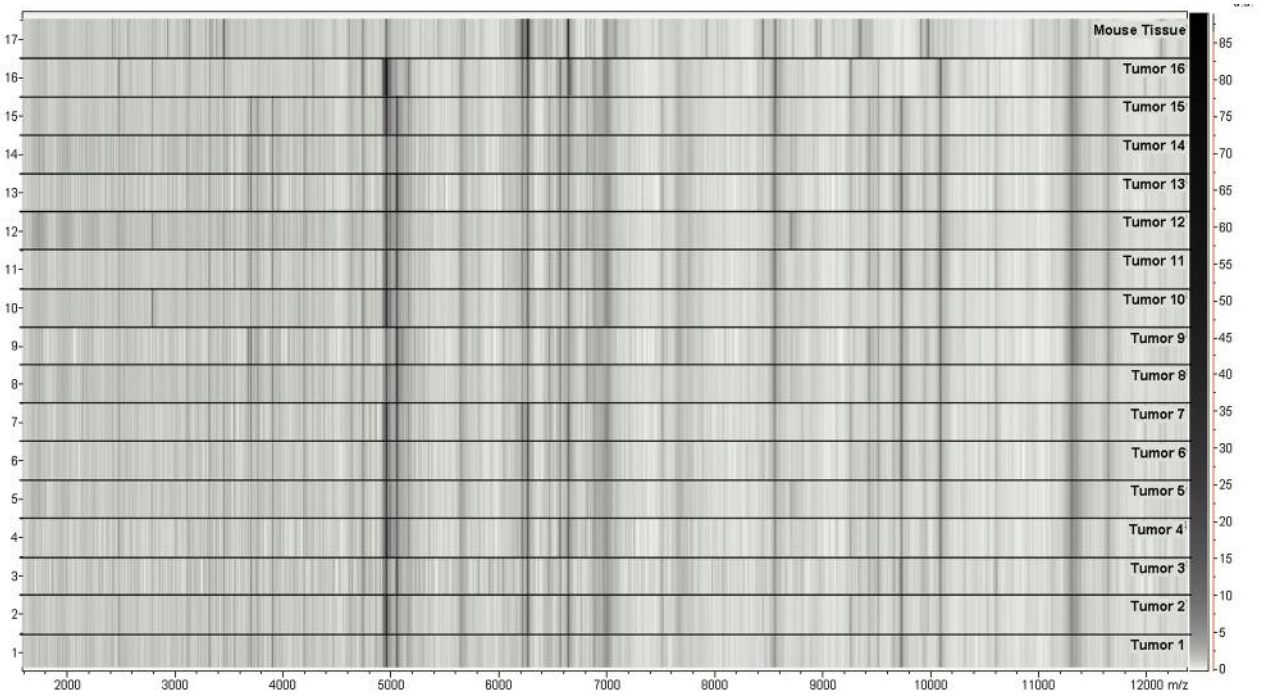

Figure 5. *Density plots of mass spectrometric imaging (MSI) spectra of diverse tumor areas and mouse tissue. Each of the 17 density plots represent the sum of the signal intensities calculated for each tumor area and for the mouse tissue (at the top).*

27). In addition, our data indicate that MSI can also be used to reveal the heterogeneous nature of tumors. It needs to be noted that in the given model system tumors were formed by an apparently homogeneous cell line. This not only underscores the relevance of using unbiased detection methods, but also the high resolving power of MSI.

An obvious limitation of MSI in comparison to classical LC-MS/MS analyses is the small number of detected signals, which is due to the absence of explicit protein-separation steps, which are necessary to reduce the complexity of the protein composition, thus reducing discriminating effects and thereby greatly increasing the yield of the number of identified proteins. Therefore, MSI only detects a small fraction of proteins (9), which cover about 1-2% of approximately 12,000 individual proteins present within an organ (11). However, our data indicate that this is sufficient to demonstrate intertumoral heterogeneity (Figures 4, 5).

The clear difference regarding the patterns of m/z signals between human tumor tissue and mouse tissue underlines the strength of MSI and can be interpreted as a proof-of-principle for the usefulness of the MSI technique. Moreover the signals are not transduction-dependent, since the fluorescent proteins have a higher molecular weight (above 26 kDa) than those detected by the mass spectrometer. However, there are also signals that were present in the spectra of both tumor and mouse tissue.

Obviously, due to relatively large interspecies genetic distance, differences in protein composition between murine and human cells were to be expected. However, as noted above, the observed heterogeneity between individual tumors derived from a cell line is quite intriguing. The obtained data indicate that even for these cell lines it might be difficult to identify single specific "cancer biomarkers" characteristic for all tumors. Instead, in order to identify each individual tumor by MSI, a panel of several biomarkers needs to be applied. Our data on the detection of tumor heterogeneity is in good agreement with a recent publication by Balluff *et al*. (2) who used MSI and statistical clustering methods to demonstrate tumor heterogeneity. Notably, application of protein panels for the detection of heterogeneous tumor cells might potentially be of special interest with regard to the detection of metastases.

In conclusion, MSI as a diagnostic tool in clinical routine for detecting and classifying cancer tissues in the future should significantly improve the quality of diagnosis. An important step towards this application of MSI is to identify tumor-specific proteomic fingerprints and to incorporate tolerances taking into account inter-individual heterogeneity.

Conflicts of Interest

The Authors declare no competing financial interests.

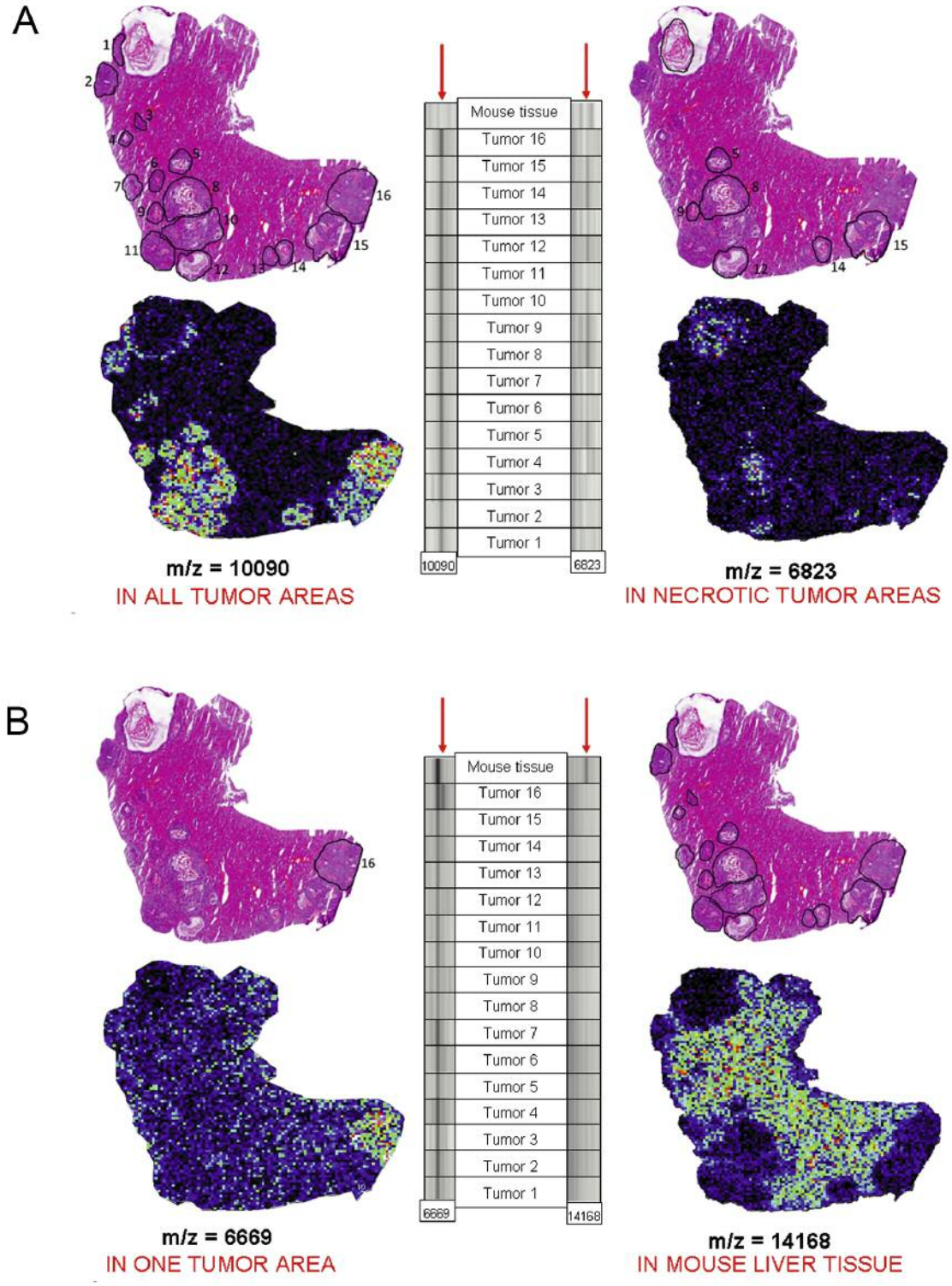

Figure 6. *Representative mass spectrometric imaging (MSI) images displaying spatial distributions of signal intensities of different m/z signals and hematoxylin and eosin (HE) staining image of the mouse liver tissue section. HE and MSI images of the mouse liver tissue sections show the distribution of tumor areas and of the signal intensities. Dark blue represent pixels on the tissue with no signal, whereas yellow and red indicate increasing signal intensities. A: The signal at 10090 m/z was detected in all tumor areas of the tissue section. In contrast, only necrotic tumor tissue contained the signal 6823 m/z. B: The signal 6669 m/z was detected exclusively in a single tumor area (tumor 16). The signal 14,168 m/z occurred in the mouse liver tissue and not in areas populated by human cancer cells.*

Acknowledgements

This work was supported in part by grants from the Forschungs- und Wissenschaftsstiftung Hamburg within the Landesexzellenzinitiative (to HS and BF), the Deutsche Forschungsgemeinschaft, DFG (SFB841/C7 to BF), an European research Advanced Grant of Dwayne Miller (HS) and the Helmholtz Society (Virtual Institute MetBioMat, HS). PA was supported by a post-doctoral grant within the Forschungsförderung Medizin program of the Medical Faculty of the University Medical Center Hamburg-Eppendorf.

Flow cytometric work was performed at the FACS Sorting Core Unit of the University Medical Center Hamburg-Eppendorf. The Authors wish to thank Christina Koop for valuable histological expertise and Svenja Linnekuhl for mouse artwork.

References

1 Ludwig JA and Weinstein JN: Biomarkers in cancer staging, prognosis and treatment selection. Nat Rev Cancer *5*: 845-856, 2005.
2 Balluff B, Frese CK, Maier SK, Schone C, Kuster B, Schmitt M, Aubele M, Hofler H, Deelder AM, Heck AJ, Hogendoorn PC, Morreau J, Maarten Altelaar A, Walch A and McDonnell LA: De novo discovery of phenotypic intratumour heterogeneity using imaging mass spectrometry. J Pathol 2014.
3 Burnum KE, Frappier SL and Caprioli RM: Matrix-assisted laser desorption/ionization imaging mass spectrometry for the investigation of proteins and peptides. Annu Rev Anal Chem *1*: 689-705, 2008.
4 Chaurand P, Norris JL, Cornett DS, Mobley JA and Caprioli RM: New developments in profiling and imaging of proteins from tissue sections by MALDI mass spectrometry. J Proteome Res *5*: 2889-2900, 2006.
5 Le CH, Han J, and Borchers CH: Dithranol as a MALDI matrix for tissue imaging of lipids by Fourier transform ion cyclotron resonance mass spectrometry. Anal Chem *84*: 8391-8398, 2012.
6 Cerruti CD, Benabdellah F, Laprevote O, Touboul D and Brunelle A: MALDI imaging and structural analysis of rat brain lipid negative ions with 9-aminoacridine matrix. Anal Chem *84*: 2164-2171, 2012.
7 Trim PJ, Henson CM, Avery JL, McEwen A, Snel MF, Claude E, Marshall PS, West A, Princivalle AP and Clench MR: Matrix-assisted laser desorption/ionization-ion mobility separation-mass spectrometry imaging of vinblastine in whole body tissue sections. Anal Chem *80*: 8628-8634, 2008.
8 Atkinson SJ, Loadman PM, Sutton C, Patterson LH and Clench MR: Examination of the distribution of the bioreductive drug AQ4N and its active metabolite AQ4 in solid tumours by imaging matrix-assisted laser desorption/ionisation mass spectrometry. Rapid Commun Mass Spectrom *21*: 1271-1276, 2007.
9 Steurer S, Borkowski C, Odinga S, Buchholz M, Koop C, Huland H, Becker M, Witt M, Trede D, Omidi M, Kraus O, Bahar AS, Seddiqi AS, Singer JM, Kwiatkowski M, Trusch M, Simon R, Wurlitzer M, Minner S, Schlomm T, Sauter Gn and Schluter H: MALDI mass spectrometric imaging based identification of clinically relevant signals in prostate cancer using large-scale tissue microarrays. Int J Cancer *133*: 920-928, 2013.
10 Cornett DS, Reyzer ML, Chaurand P and Caprioli RM: MALDI imaging mass spectrometry: molecular snapshots of biochemical systems. Nat Methods *4*: 828-833, 2007.
11 Wilhelm M, Schlegl J, Hahne H, Moghaddas Gholami A, Lieberenz M, Savitski MM, Ziegler E, Butzmann L, Gessulat S, Marx H, Mathieson T, Lemeer S, Schnatbaum K, Reimer U, Wenschuh H, Mollenhauer M, Slotta-Huspenina J, Boese JH, Bantscheff M, Gerstmair A, Faerber F and Kuster B: Mass-spectrometry-based draft of the human proteome. Nature *509*: 582-587, 2014.
12 Weber K, Thomaschewski M, Warlich M, Volz T, Cornils K, Niebuhr B, Tager M, Lutgehetmann M, Pollok JM, Stocking C, Dandri M, Benten D and Fehse B: RGB marking facilitates multicolor clonal cell tracking. Nat Med *17*: 504-509, 2011.
13 Weber K, Thomaschewski M, Benten D and Fehse B: RGB marking with lentiviral vectors for multicolor clonal cell tracking. Nat Protoc *7*: 839-849, 2012.
14 Weber K, Bartsch U, Stocking C and Fehse B: A multicolor panel of novel lentiviral 'gene ontology' (LeGO) vectors for functional gene analysis. Mol Ther *16*: 698-706, 2008.
15 Prochazka M, Gaskins HR, Shultz LD and Leiter EH: The nonobese diabetic scid mouse: model for spontaneous thymomagenesis associated with immunodeficiency. Proc Natl Acad Sci USA *89*: 3290-3294, 1992.
16 Custer RP, Bosma GC and Bosma MJ: Severe combined immunodeficiency (SCID) in the mouse. Pathology, reconstitution, neoplasms. Am J Pathol *120*: 464-477, 1985.
17 Shaner NC, Campbell RE, Steinbach PA, Giepmans BN, Palmer AE and Tsien RY: Improved monomeric red, orange and yellow fluorescent proteins derived from Discosoma sp. red fluorescent protein. Nat Biotechnol *22*: 1567-1572, 2004.
18 Nagai T, Ibata K, Park ES, Kubota M, Mikoshiba K and Miyawaki A: A variant of yellow fluorescent protein with fast and efficient maturation for cell-biological applications. Nat Biotechnol *20*: 87-90, 2002.
19 Rizzo MA, Springer GH, Granada B and Piston DW: An improved cyan fluorescent protein variant useful for FRET. Nat Biotechnol *22*: 445-449, 2004.
20 Fehse B, Kustikova OS, Bubenheim M and Baum C: Pois(s)on-it's a question of dose. Gene Ther *11*: 879-881, 2004.
21 Townsend CM, Jr., Ishizuka J, and Thompson JC: Studies of growth regulation in a neuroendocrine cell line. Acta Oncol *32*: 125-130, 1993.
22 Cornils K, Thielecke L, Huser S, Forgber M, Thomaschewski M, Kleist N, Hussein K, Riecken K, Volz T, Gerdes S, Glauche I, Dahl A, Dandri M, Roeder I and Fehse B: Multiplexing clonality: combining RGB marking and genetic barcoding. Nucleic Acids Res *42*: e56, 2014.
23 Moll R, Franke WW, Schiller DL, Geiger B and Krepler R: The catalog of human cytokeratins: patterns of expression in normal epithelia, tumors and cultured cells. Cell *31*: 11-24, 1982.
24 Shen J, Person MD, Zhu J, Abbruzzese JL and Li D: Protein expression profiles in pancreatic adenocarcinoma compared with normal pancreatic tissue and tissue affected by pancreatitis as detected by two-dimensional gel electrophoresis and mass spectrometry. Cancer Res *64*: 9018-9026, 2004.
25 Chaurand P, Stoeckli M, and Caprioli RM: Direct profiling of proteins in biological tissue sections by MALDI mass spectrometry. Anal Chem *71*: 5263-5270, 1999.
26 Zheng Y, Xu Y, Ye B, Lei J, Weinstein MH, O'Leary MP, Richie JP, Mok SC and Liu BC: Prostate carcinoma tissue proteomics for biomarker discovery. Cancer *98*: 2576-2582, 2003.
27 Stoeckli M, Chaurand P, Hallahan DE and Caprioli RM: Imaging mass spectrometry: a new technology for the analysis of protein expression in mammalian tissues. Nat Med *7*: 493-496, 2001.

Received April 14, 2015
Revised May 18, 2015
Accepted May 20, 2015